FLSEVIER

Contents lists available at ScienceDirect

Science of the Total Environment





Simulating the impact of gas-wall partitioning on SOA formation using the explicit gas mechanism integrated with aqueous reactions containing electrolytes



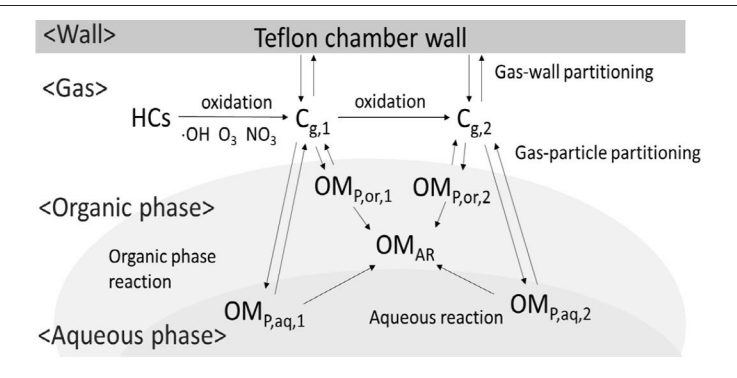
Sanghee Han, Myoseon Jang*

Department of Environmental Engineering Science, University of Florida, Gainesville, FL, USA

HIGHLIGHTS

- Prediction of SOA formation via multiphase reactions of hydrocarbons
- Gas-wall partitioning model based on qualitative structure activity relationship
- The impact of gas-wall partitioning on SOA formation under varying NO_x and seeds

GRAPHICAL ABSTRACT



ARTICLE INFO

Article history: Received 20 May 2020 Received in revised form 25 July 2020 Accepted 27 July 2020 Available online 7 August 2020

Editor: Pingqing Fu

Keywords:
Gas-wall partitioning
SOA model
Quantitative structure activity relationship
Explicit mechanisms
Aqueous reactions

ABSTRACT

The impact of the Teflon reactor wall on secondary organic aerosol (SOA) formation was explicitly simulated by using the Unified Partitioning Aerosol Phase Reaction (UNIPAR) model integrated with gas-wall partitioning (GWP). The formation of oxygenated semivolatile organic compounds (SVOCs) from the photooxidation of hydrocarbons (HC) was simulated by using an explicit gas-kinetic mechanism (MCM V3.3.1). In the model, SVOC's GWP and gas-particle partitioning onto preexisting particulate matter were kinetically treated with the absorption and desorption processes. The UNIPAR model streamlined aerosol growth via the oligomerization of reactive SVOCs in the organic phase and aqueous reactions in the inorganic phase. Two important GWP parameters, GWP coefficient $(K_{w,i})$ and the deposition rate constant $(k_on_{w,i})$ of SVOCs (i) to the wall were predicted by using a quantitative structure activity relationship (QSAR) employing SVOCs' physicochemical descriptors. This GWP model was then incorporated with the UNIPAR model in the DSMACC-KPP platform and simulated SOA chamber data. The three different HCs (toluene, 1,3,5-trimethylbenzene, and α -pinene) were photochemically oxidized in the presence of NO_x and inorganic seed aerosols in an outdoor photochemical smog chamber (UF-APHOR). The impact of GWP on SOA mass varied ranging from 9% to 71% with HCs, seed conditions, NO_x, and temperature. Toluene SOA in the absence of inorganic aerosol was the most sensitive to GWP. However, in the presence of wetinorganic seed, the impact of GWP on SOA was smaller than that of non-seed SOA owing to rapid reactions of organic species in the aqueous phase. SOA mass can be significantly underestimated in the absence of wetinorganic seed when the aerosol model employs parameters derived using SOA data with GWP artifacts.

© 2020 Elsevier B.V. All rights reserved.

* Corresponding author. E-mail address: mjang@ufl.edu (M. Jang).

1. Introduction

Secondary Organic Aerosol (SOA), formed by oxidation of hydrocarbons (HCs), accounts for a significant fraction (ranging from 20% to 90%) of organic aerosol in the ambient air (Hallquist et al., 2009; Tsigaridis et al., 2014). This SOA can considerably influence climate (Seinfeld and Pandis, 2016) and human health (Cohen et al., 2017; Pöschl, 2005). Thus, models to estimate the SOA burden in regional and global scales has been developed (Carlton et al., 2009; Tsigaridis et al., 2014; Barsanti et al., 2017). SOA model parameters are typically derived based on observed data using laboratory studies. However, the predicted SOA mass in the regional scale has been underestimated compared to field data (Ensberg et al., 2014; Tsigaridis et al., 2014). For example, the Community Multi-scale Air Quality Model (CMAQ) tends to underestimate SOA mass, particularly during summer seasons (Appel et al., 2017; Zhang et al., 2014a). Missing precursors and reaction mechanisms have been suggested as main reasons for the low predicted SOA mass (Barsanti et al., 2013). For the last two decades, a significant effort has been placed on studies of aerosol phase chemistry to identify missing SOA formation mechanisms. For example, the formation of nonvolatile oligomers in the aerosol phase is known to significantly attribute to SOA production. Thus, the addition of in-particle chemistry into SOA models has been attempted in several aerosol models (Jang et al., 2002; McNeill et al., 2012; Beardsley and Jang, 2016; Im et al., 2014). Additionally, the autoxidation pathway in gas mechanisms has recently been reported to form condensable high molecular weight products in terpene SOA (Bianchi et al., 2019).

Gas-Wall Partitioning (GWP) of semivolatile organic compounds (SVOCs) to the reactor surface can compete with gas-particle partitioning and lead to the negative bias of the SOA formation. For example, Matsunaga and Ziemann reported that 3-57% of total concentration of n-alkanes and 1-alkenes was deposited to the chamber wall (Matsunaga and Ziemann, 2010). The study of GWP has been extended to various functionalities, such as alcohols, mono-carboxylic acids, multi alcohols, alkylnitrates, and hydroxy nitrates (Krechmer et al., 2016; Yeh and Ziemann, 2014, 2015). The observations from these chamber studies showed that 1% to 97% of total SVOCs were able to partition to the reactor wall. In order to predict GWP, vapor pressure of SVOCs (i) or vapor saturation concentration were typically used. However, SVOC's GWP is also influenced by the activity coefficient ($\gamma_{w,i}$) of SVOC in organic matter (OM_{wall}) on the surface of the chamber wall. The $\gamma_{w, i}$ value is set to unit (one) in most of the GWP model. However, $\gamma_{w,i}$ can vary depending on the chemical properties (i.e., polarity and molecular size) of SVOCs and influence on the GWP coefficient of $i(K_{w,i})$ (Huang et al., 2018; Krechmer et al., 2016). In our recent study, the explicit-structure based GWP model was attempted by the quantitative structureactivity relationship (QSAR) for the prediction of $K_{w,i}$ and the absorption rate constant $(k_{-}on_{w,i})$ (Han et al., 2019). To predict $K_{w,i}$ and $k_{-}on_{w, i}$, a polynomial equation was semiempirically derived by fitting the coefficients of physicochemical parameter terms for various SVOCs to chamber data (n-alkanes, aliphatic alcohols, carboxylic acids, aldehydes, phenols, ketones) under different relative humidity (RH) conditions (RH: 40-75%).

The preexisting SOA models based on partitioning use two surrogate products (Odum et al., 1996) or several semivolatile surrogates (e.g., VBS) (Donahue et al., 2006) with semi-empirical parameters (mass-based stoichiometric coefficient and gas-particle partitioning coefficient) for a given HC system. Due to its simplicity and efficiency, the two-product model has been widely used in regional and global models (Carlton et al., 2009; Volkamer et al., 2006; Barsanti et al., 2017). Nevertheless, the two-product model and its predecessors are limited in their ability to predict SOA formation from GWP, which needs to be explicitly predicted based on the chemical properties of oxidized products. To date, only a few studies attempted to explicitly predict the impact of GWP on SOA mass considering SVOC's chemical structure. For example, (La et al., 2016) explicitly simulated the GWP and applied it to the

prediction of SOA mass from the photooxidation of alkanes and aliphatic-alkenes utilizing the Generator for Explicit Chemistry and Kinetics of the Organics in the Atmosphere (GECKO-A) model. Their model evaluated that the SOA yields can be underestimated by more than 50% due to the GWP bias. Zhang's study reported that the significance of the GWP factor on SOA mass ranged from 1.1 to 4.2 utilizing the statistical oxidation model (SOM), which simulated the kinetic process of hydrocarbon. (Zhang et al., 2014b). In SOM, the GWP was dynamically modeled with the empirical GWP parameters (i.e., OM_{wall} , vapor-wall deposition rate constant, and vapor saturation concentration) obtained from chamber studies. Cappa et al. corrected the SOM for GWP at two different levels and integrated it into the UCD/CIT chemical-transport model for the SOA mass prediction at the regional scale (Cappa et al., 2016). However, the uncertainty of the prediction of SOA mass was significant owing to a large variation in GWP. For example, the predicted SOA mass substantially increased by factors of \sim 2–5 for the low and \sim 5–10 for the high GWP scenarios.

Moreover, aerosol phase reactions of organic products are important pathways to form SOA because they yield nonvolatile oligomeric matter. The formation of oligomeric matter is further accelerated by an acid-catalyst such as sulfuric acid in the presence of wet inorganic seed aerosol (Beardsley and Jang, 2016; Hallquist et al., 2009; Im et al., 2014; Jang et al., 2002; Tolocka et al., 2004; Zhou et al., 2019). However, typical partitioning-based SOA models are limited in their ability to predict SOA formation from in-particle chemistry in the presence of the inorganic aqueous phase due to the loss of individual product structures, which determine SVOC's reactivity in the aerosol phase. To accurately predict SOA formation via multiphase reactions without GWP artifacts, the development of a state-of-the-art science model that uses the explicit structure of oxygenated products originating from gas-phase oxidation of HCs is necessary. The Unified Partitioning Aerosol Phase Reaction (UNIPAR) model was semi-empirically developed, and simulated the SOA formation via multiphase processes such as gas oxidation, gas-particle partitioning, and aerosol phase reaction (Beardsley and Jang, 2016; Im et al., 2014; Zhou et al., 2019). The UNIPAR model explicitly treated gas-phase oxidation as a kinetic mechanism (MCM v.3.3.1) (Jenkin et al., 2012). The UNIPAR model employs a lumping structure based on the volatility of the oxidized products and reactivity in the aerosol phase reaction and predicts the SOA formation while accounting for the mass balance-based gas-partitioning and in-particle chemistry to form oligomers.

In this study, the UNIPAR-GWP model was newly developed by coupling the UNIPAR model with the QSAR based GWP model to predict SOA mass without the wall artifacts. In the model, partitioning of gaseous oxygenated compounds in multiphase (including the gas phase, organic aerosol phase, inorganic aerosol phase, and the wall phase) was explicitly treated using the kinetic process. The dynamically predicted concentrations of oxidized products in each phase were applied to gas phase aging of products and heterogeneous reactions in the aerosol phase. The UNIPAR-GWP model was evaluated by comparing the predicted SOA mass with the observed SOA created from three different hydrocarbons (toluene, 1,3,5-trimethylbenzene, and α -pinene) in the presence of NO_x using a large outdoor photochemical reactor. The UNIPAR-GWP model contributions to a more in-depth understanding of the impact of the reactor wall on SOA production are as follows. (1) Owing to the inclusion of both GWP and aerosol phase reaction modules, the SOA formation via aqueous phase reaction was evaluated without GWP bias. (2) The sensitivity of SOA formation to the major SOA model variables (temperature, RH, NO_x levels, and type of seed) was studied in the absence of GWP bias. (3) The significance of SVOC's major pathways, such as GWP, gas-particle partitioning, and aerosol phase reactions was evaluated. (4) The model of this study enabled in-depth understanding of chamber specific parameters (i.e., surface area to volume (A/V) ratio of the chamber and OM_{wall}) for SOA formation. The resulting model of this study will allow to predict the impact of GWP on different chambers. Ultimately, the study using UNIPAR- GWP will permit the improvement of predictions of SOA burdens in regional scales.

2. Experimental section

The chamber experiments to produce the GWP model and SOA formation were conducted in the University of Florida Atmospheric PHotochemical Outdoor Reactor (UF-APHOR) chamber located on the rooftop of Black Hall (29.64, -82.34) at the University of Florida, Gainesville, Florida. The configuration of the UF-APHOR and the experimental procedure were reported in previous studies (Beardsley and Jang, 2016; Im et al., 2014; Zhou et al., 2019) in detail.

2.1. Chamber experiments to develop the GWP model

In order to predict GWP, the estimation of both $K_{w, i}$ and $k_on_{w, i}$ are essential (see Section 3.1). The detail information about the chamber experiments to develop GWP model is described in Section S1 of supplementary. Supplementary table S1 summarizes the experimental conditions of the chamber experiments using the UF-APHOR chamber to develop the GWP model. The predictive models for $K_{w,i}$ and $k_on_{w,i}$ for various SVOCs (listed in Table S2) are semiempirically obtained based on the time series measurements of gas phase SVOCs. The relative humidity (RH) was controlled at three different levels (40–53, 75, 85) during the chamber experiments to develop an RH-dependent GWP model. The detailed information of the chemical injection and the workup procedure for chemical analysis of gaseous SVOCs is in our previous study (Han et al., 2019) and is described in the Section S1.1 of supplementary. In brief, GWP experiments were performed during the nighttime to avoid any photochemical reaction. The cocktail of SVOCs was introduced to the chamber and the SVOC vapor was sampled 13 times during the experiment using a 40-cm 5-channel annular denuder coated with XAD-4 resin powder (Gundel et al., 1995; Leach et al., 1999). The gas chromatography/mass spectrometer (GC/MS) (Varian 3800/2000 GC/MS, Palo Alto, CA, USA) was used to analyze the concentration of each SVOC compound in the solvent extracted samples. The scanning mobility particle sizer (SMPS, TSI 3080, Shoreview, MN, USA) and a condensation particle counter (CPC, TSI 3022A, Shoreview, MN, USA) sampled the particle concentration during the experiment to ensure that there was no particle formation during the experiment.

2.2. Chamber experiments to form SOA

SOA was produced from the photooxidation of three different hydrocarbons (toluene (Tol), 1,3,5-trimethylbenzene (TMB), and α pinene (AP)) in the presence of NO_x in the UF-APHOR (Table 1) under ambient sunlight. The experiments began at sunrise and were conducted for 12 h. The in situ measurement of HCs, trace gases (O₃, SO₂, and NO_x), inorganic ions, and organic carbon (OC) of particles was monitored, as well as meteorological factors (i.e., relative humidity; temperature; and ultraviolet radiation) in the UF-APHOR. Aerosol acidity (mol/ L of aerosol) is monitored using colorimetry integrated with the reflectance UV-visible spectrometer (C-RUV) technique (Li et al., 2016; Jang et al., 2020). In order to investigate the NO_x effect on SOA formation, two different NO_x levels (high-NO_x: HC/NO_x (ppbC/ppb) < 5.5; low- NO_x : HC/NO_x (ppbC/ppb) > 5.5) were applied. Several sets of experiments were conducted with electrolytic seed aerosols (i.e., sulfuric acid, SA; or wet ammonium sulfate, wAS) to evaluate the wet-seed effect on the SOA formation. HONO was additionally injected into the toluene SOA system as a reaction initiator. The ratio of organic matter (OM) to OC was experimentally determined as 1.9 (Zhou et al., 2019) and 1.7 (from experiment on 8/28/2019) for the aromatic and terpene systems, respectively.

3. Model descriptions

Fig. 1 illustrates the overall structure of the UNIPAR-GWP model. In this model, QSAR based GWP was integrated into the UNIPAR model. The concentration of oxygenated products originating from oxidation of HCs is explicitly predicted by using MCM (v.3.3.1) (Jenkin et al., 2012). The multiphase partitioning of organic products between the gas phase, organic aerosol phase, inorganic aerosol phase, and the wall phase were kinetically treated by using the absorption and desorption rate constants. UNIPAR also processes the heterogeneous reactions of organic compounds partitioned in the organic aerosol phase and aqueous reactions in the inorganic aerosol phase. The aqueous reactions of organic compounds can also be accelerated by an acid catalyst.

3.1. GWP model

The GWP of SVOCs (i) is treated as deposition–evaporation kinetics in the model. This partitioning process of i into organic matter on the Teflon wall (OM_{wall}) can be expressed as:

$$SVOC_{g,i} \xrightarrow{k_on_{w,i}} SVOC_{w,i}$$
 (1)

$$SVOC_{w,i} \xrightarrow{k_off_{w,i}} SVOC_{g,i}$$
 (2)

in which $k_on_{w,i}$ and $k_off_{w,i}$ are deposition rate constant and evaporation rate constant of i, respectively. GWP is assumed as a partitioning process of gaseous SVOCs into OMwall, reflecting the characteristic of the outdoor chamber of this study. OM_{wall} was obtained by analyzing the organic matter using Fourier-transform infrared spectroscopy (FTIR) spectra. OM_{wall} is obtained by extracting the Teflon film surface with organic solvents (i.e., dichloromethane and ethyl acetate). In FTIR spectra (supplementary Fig. S1), the aliphatic functionality (C—H stretching bend) is dominant, and oxygenated functionalities such as carbonyl, alcohols, and carboxylic acid are minor. The air in the UF-APHOR chamber is ventilated after each chamber experiment by being exposed to ambient air for several hours and cleaned using the clean air generator for two days. Thus, the chamber wall can be influenced by trace compounds in ambient air during the ventilation procedure. Long chain *n*-alkanes (wax-like matter) are common in ambient air due to primary emissions (combustion of fossil fuels) and biogenic emissions (Bi et al., 2003; Simoneit, 1989; Lyu et al., 2019). The Teflon film (Fluorinated Ethylene Propylene (FEP) Teflon film) is generally very hydrophobic. Its solubility parameter, based on Hansen's parameter (Barton, 2017), is even lower than alkanes and more favorable to the adsorption of wax-like alkanes than oxygenated organic compounds. Furthermore, the oxidation of long-change alkanes is generally slower than oxygenated compounds such as aldehydes, and this tendency increases the hydrophobicity of the wax-like OMwall.

The equilibrium constant (K_{eq}) of GWP is theoretically calculated as the conventional partitioning coefficient expressed as below:

$$K_{eq} = \frac{7.501RT}{10^9 MW_{OM} \gamma_{w,i} p_{L,i}^{\circ}} = \frac{kon_{w,i}}{kof f_{w,i} OM_{wall}}$$
(3)

R is the ideal gas constant (8.314 J mol $^{-1}$ K $^{-1}$) and T is the temperature (K). MW_{OM} is OM_{wall} 's average molecular weight, and $p_{L,i}$ is the liquid vapor pressure (mmHg) of SVOC(i). OM_{wall} (18.52 mg m $^{-3}$) is the concentration of the OM_{wall} in the chamber, determined based on the measurement. The unitless GWP coefficient ($K_{w,i}$) is determined by multiplying OM_{wall} by the K_{eq} :

$$K_{w,i} = K_{eq}OM_{wall} = \frac{7.501RTOM_{wall}}{10^9 MW_{OM} \gamma_{w,i} p_{L,i}^{\circ}}$$
(4)

Table 1The chamber experimental data to investigate the impact of GWP on SOA formation. The experiments were performed in the presence of NO_x and inorganic-seeded aerosol under ambient sunlight by using the UF APHOR chamber.

НС	NO _x condition	Seed Condition ^a	Date	Initial HC conc. (ppb)	Initial NO conc. (ppb)	Initial NO ₂ conc. (ppb)	Initial HONO conc.(ppb)	HC/NO _x (ppbC/ppb)	$OM_0^b \ (\mu g/m^3)$	SOA Yield (%) ^c	RH (%)	Temp. (K)	Note.
		NS	6/20/2012	165	64	2	11	15.00	5	13	27-83	295-317	Fig. 1a
	Low-NO _x	SA	6/20/2012	165	90	5	15	10.50	5	15.6	27-83	295-317	Fig. 1a
toluono		SO_2	1/6/2012	190	35	35	40	12.09	5	18.9	18-81	280-306	Fig. S4a
toluene		NS	2/9/2012	180	180	31	35	4.52	4	9.3	21-84	280-307	Fig. 1d
	High-NO _x	SO_2	2/9/2012	175	180	30	35	5	4	15.3	21-83	280-307	Fig. S4b
		SA	4/30/2018	127	295	10	47	2.9	2	13.1	14-57	289-317	Fig. 1d
	Low-NO _x	NS	9/7/2019	210	102	25	0	14.9	1	2.0	10-39	294-323	Fig. 1b
		SA	9/7/2019	200	101	26	0	14.2	1	5.4	20-49	294-319	Fig. 1b
TMB		wAS	9/19/2019	210	97	15	0	16.9	1	4.4	26-74	298-320	Fig. S4c
IIVID		NS	9/10/2019	210	532	69	0	3.1	1	1.1	13-40	296-322	Fig. 1e
	High-NO _x	SA	9/10/2019	210	546	71	0	3.1	1	3.4	23-50	297-319	Fig. 1e
		SO_2	5/20/2012	160	195	48	75	5.2	4	7.3	14-95	290-317	Fig. S4d
		NS	8/28/2019	124	100	9.4	0	11.3	4	6.1	14-40	296-320	Fig. 1c
	Low-NO _x	SA	8/28/2019	130	101	9.4	0	11.8	4	12.3	32-54	296-317	Fig. 1c
a-pinene		wAS	7/30/2019	117	50	23	0	16.0	6	10.3	31-84	273-321	Fig. S4e
	High NO	NS	7/18/2019	140	169	136	0	4.6	3	6.5	19-48	294-319	Fig. 1f
	High-NO _x	SA	7/18/2019	140	148	156	0	4.6	4	11.4	13-42	294-320	Fig. 1f

^a Seed condition defines the injected electrolytic seed condition. NS, SA, SO₂, and wAS denote the non-seed, sulfuric acid, SO₂, and wAS (RH > ERH) seeded condition, respectively.

 $K_{w, i}$ can be defined as $k_on_{w, i}$ to $k_off_{w, i}$ ratio. By taking the logarithm of Eq. (4), $K_{w, i}$ can be expressed as:

$$\ln\left(K_{w,i}\right) = -\ln\left(\gamma_{w,i}\right) - \ln\left(p_{L,i}^{\circ}\right) + \ln\left(\frac{7.501RTOM_{wall}}{10^{9}MW_{OM}}\right)$$
 (5)

 $k_on_{w,\,i}$ is defined as a fractional loss rate with the accommodation coefficient of i to the wall $\alpha_{w,\,i}$, (McMurry and Grosjean, 1985) expressed as:

$$k_on_{w,i} = \left(\frac{A}{V}\right) \frac{\alpha_{w,i} \bar{v}_i / 4}{1 + \frac{\pi \alpha_{w,i} \bar{v}_i}{8\sqrt{K_e D}}} \tag{6}$$

 \overline{v}_i is the gas molecules' mean thermal speed. $D (1.0 \times 10^{-6} \text{ m}^2 \text{ s}^{-1})$ and $K_e (0.12 \text{ s}^{-1})$ are referred to as the diffusion coefficient and coefficient of eddy diffusion applied as a fixed number, respectively.

The QSAR theory is frequently used to predict the solvent effect on the reaction rate constants or equilibrium constants in the form of a linear solvation energy relationship (Alan, 1992; Puzyn et al., 2010). In environmental studies, the partitioning of an organic compound in airborne particles was predicted by applying the QSAR (Arp and Goss, 2009; Endo and Goss, 2014; Salthammer and Goss, 2019; Jang and Kamens, 1999). In the QSAR approach, $\alpha_{w,i}$ and $\gamma_{w,i}$ can be expressed as below and apply to the QSAR equation coupled with their physicochemical parameters because of their structure reliability.

$$\ln (K_{w,i}) = -(a_p H_{d,i} + b_p H_{a,i} + r_p \alpha_i + c_p) - \ln (p_{L,i}^{\circ})
+ \ln \left(\frac{7.501RTOM_{wall}}{10^9 MW_{OM}}\right)$$
(7)

$$\ln(\alpha_{w,i}) = a_d H_{d,i} + b_d H_{d,i} + s_d S_i + r_d \alpha_i + c_d$$
(8)

where $H_{d,i}$, $H_{a,i}$, S_i , and α_i indicate the hydrogen bond donor, hydrogen bond acceptor, dipolarity/polarizability, and polarizability, respectively (Abraham and McGowan, 1987; Abraham et al., 1991; Platts et al., 1999)

In this study, QSAR models are semiempirically determined by using the experimental data that measured time series gas-phase

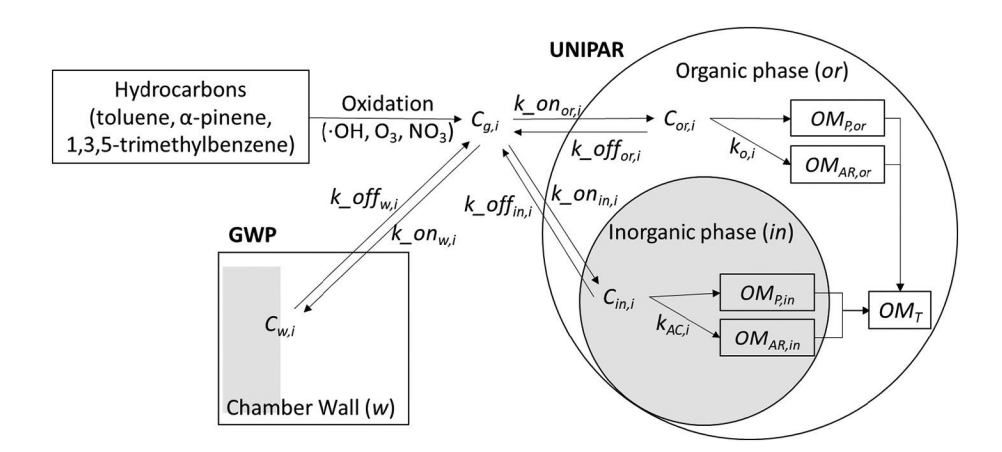


Fig. 1. The structure of the UNIPAR-GWP explicit model to predict the impact of gas-wall partitioning on SOA formation. C denotes the concentration of organic compound (i) in gas phase (g), organic phase (in), inorganic phase (in), and chamber wall phase (w). The gas-wall and gas-particle partitioning coefficients of i are integrated by using k_on (absorption rate constant) and k_off (desorption rate constant) between gas phase (g) and three phases (or, in, and w). k_{oi} and k_{ACi} are the rate constants of oligomerization of i in or and in in, respectively. C_{gi} is simulated using the gas kinetic mechanisms (MCM v3.3.1, Jenkin et al., 2012). The partitioning process is kinetically treated by using k_on and k_off . Aerosol phase reactions of i are processed by using the UNIPAR module. The gas phase reaction, multiphase partitioning processes and aerosol phase reactions to form SOA mass are integrated into chemical solver.

^b OM₀ is pre-existing organic matter in the chamber. It is determined based on the organic matter concentration of background sample.

 $^{^{\}rm c}$ SOA yield is estimated by generated organic mass ($\mu {\rm g~m^{-3}}$) to consumed hydrocarbon ($\mu {\rm g~m^{-3}}$) ratio.

concentrations of SVOCs in the UF-APHOR chamber to predict $K_{w,i}$ and $\alpha_{w,i}$, respectively:

$$\ln\left(K_{w,i}\right) = -\left(2.25^{0.0007RH}H_{d,i} + 0.79^{0.022RH}H_{d,i} + 0.14^{0.0025RH}\alpha_{i} - 6.54^{0.0047RH}\right)$$

$$-\ln\left(p_{L,i}^{\circ}\right) + \ln\left(\frac{7.501RTOM_{wall}}{10^{9}MW_{OM}}\right) \tag{9}$$

$$\ln\left(\alpha_{w,i}\right) = -0.33H_{d,i} - 3.00H_{d,i} - 0.05\alpha_i - 0.61S_i - 9.69\tag{10}$$

The QSAR equations (Eqs. (9) and (10)) are determined based on the statistical evaluation described in the Section S1.2. RH dependency of the coefficient in the $K_{w,i}$ predictable QSAR equation is determined based on the chamber studies under three different RHs (supplementary Fig. S2). In supplementary Fig. S3, the predicted and observed ln $(K_{w,i})$ shows descent linearity (y = 0.97×, R² = 0.80). k_on_{w,i} is determined by substituting the $\alpha_{w,i}$ predicted by polynomial equation (Eq. (10)) to the Eq. (6). k_off_{w,i} is calculated by dividing k_on_{w,i} with $K_{w,i}$ predicted by the QSAR polynomial equation (Eq. (9)).

3.2. UNIPAR-GWP model

The UNIPAR model treats the oxidized products as a 51 lumped arrays with eight levels of volatility $(1-8:10^{-8},10^{-6},10^{-5},10^{-4},10^{-3},10^{-2},10^{-1},$ and 1 mmHg) and six levels of aerosol-phase reactivity (very fast: VF, fast: F, medium: M, slow: S, partitioning only: P, and multi-alcohol: MA) and three additional reactive species (glyoxal (GLY), methylglyoxal (MGLY), and epoxydiols (IEPOX)). The UNIPAR-GWP model treats vapor pressure and aerosol-phase reactivity of the oxidized products as lumped groups while all other model parameters (the organic to carbon ratio (O:C), molecular weight (MW), H-bonding (HB), and activity coefficients in inorganic $(\gamma_{in,i})$) were explicitly treated by using actual molecular structure. The UNIPAR model is incorporated with GWP that are explicitly treated using the QSAR-model predicted $k_{-On_{w,i}}$ and $k_{-Off_{w,i}}$. The UNIPAR-GWP model was simulated using a chemistry box model platform, the Dynamically Simple Model for Atmospheric Chemical Complexity (DSMACC).

The partitioning processes were treated using absorption-desorption kinetics and incorporated with gas-kinetic mechanisms to dynamically treat GWP in a similar way to Eqs. (1) and (2) using the absorption $(k_on_{or,i} \text{ or } k_on_{in,i})$ and desorption rate constant $(k_off_{or,i} \text{ or } k_off_{in,i})$ between the gas and particle phase (or: organic, in: inorganic). $k_on_{or,i}$ and $k_on_{in,i}$ were defined based on the flux equation of condensable organic species from the gas phase to an aerosol particle of diameter D_p (100 nm) (Bowman et al., 1997; Wexler and Seinfeld, 1990) below:

$$k_on_{or,i} = \frac{2\pi D_p \lambda \overline{c} \left(C_{g,i} - C_{g,i}^{eq} \right)}{1 + 8\lambda / \alpha_{or} D_p} \tag{11}$$

$$k_on_{in,i} = \frac{2\pi D_p \lambda \overline{c} \left(C_{g,i} - C_{g,i}^{eq} \right)}{1 + 8\lambda / \alpha_{in} D_n}$$
(12)

where $C_{g,i}$ and $C_{g,i}^{eq}$ are the bulk gas-phase concentrations ($\mu g m^{-3}$) of i and that in the equilibrium state, respectively. The impact of the Kelvin effect on G_i^{eq} is neglected for the particle size larger than 0.1 μm . λ (μm) is the mean free path of air, and \bar{c} ($m s^{-1}$) is the mean molecular speed of SVOC (i). α_{or} and α_{in} are the accommodation coefficients of SVOC(i) to the organic phase and inorganic phase, respectively. The equilibrium of gas-particle partitioning is rapidly established assuming the perfect accommodation of organic vapors onto particles ($\alpha_{or} = \alpha_{in} = 1$) (Julin et al., 2014). The seed surface area was not considered based on the assumption that accommodation of organic vapors onto particles is perfect without substantial limitations to vapor-particle mass transfer (Nah

et al., 2016). The gas-particle partitioning coefficient in the organic phase and the inorganic phase are described as $K_{or,i}$ and $K_{in,i}$ (Pankow, 1994; Beardsley and Jang, 2016; Im et al., 2014; Zhou et al., 2019)

$$K_{or,i} = \frac{7.501RT}{10^9 MW_{or} \gamma_{or,i} p_{L,i}^{\circ}}$$
 (13)

$$K_{in,i} = \frac{7.501RT}{10^9 MW_{in} \gamma_{in,i} p_{L,i}^{\circ}}$$
 (14)

 $\gamma_{or,i}$ is the activity coefficient of SVOC in or phase and $\gamma_{or,i}$ is assumed as unity. $\gamma_{in,i}$ is semi-empirically estimated by a polynomial equation, by fitting the theoretically estimated $\gamma_{in,i}$ (AIOMFAC (Zuend et al., 2011)) of model organic compounds to RH, O:C, MW, HB, and fractional sulfate (FS) of i (Zhou et al., 2019):

$$\gamma_{in,i} = e^{0.035MW_i - 2.704 \ln(0.C_i) - 1.121HB_i - 0.330FS - 0.022RH}$$
(15)

 $\gamma_{in,i}$ for different SOA systems is discussed in Section 4.3. $k_off_{or,i}$ and $k_off_{in,i}$ are obtained from absorption rate constants ($k_on_{or,i}$ and $k_on_{in,i}$), the partitioning coefficient of SVOCs ($K_{or,i}$ and $K_{in,i}$), and aerosol concentrations (OM_T and M_{in}):

$$koff_{or,i} = \frac{kon_{or,i}}{K_{or,i}OM_T} \tag{16}$$

$$koff_{in,i} = \frac{kon_{in,i}}{K_{in,i}M_{in}} \tag{17}$$

where OM_T (µg m⁻³) is total concentration of organic matter and M_{in} ($\mu g m^{-3}$) is the concentration of inorganic aerosol. OM_T is the sum of the concentration of organic matter produced from gas-particle partitioning (OM_P) of oxidized products and the OM produced by aerosol phase reaction (OM_{AR}). The OM_{AR} formation includes the oligomerization in the organic phase and aqueous reaction in the inorganic phase, following the previous studies (Im et al., 2014; Zhou et al., 2019). OM_{AR} is estimated by analytical solution of the second-order kinetic dimerization reaction (Odian, 2004) based on the aerosol-phase reactivity scales of lumping groups. Oligomerization in an aqueous phase can be accelerated by inorganic acid via acid-catalyzed reactions of reactive organic species (Jang et al., 2002). The oligomerization rate constant $(k_{AC,i})$ in the aqueous phase is determined by a semiempirical model developed by (Jang et al., 2005) as a function of reactivity scale (R_i) , protonation equilibrium constant (pK_{BH+i}) , excess acidity (X), water activity (a_w) , and proton concentration ([H⁺]), estimated by using the inorganic thermodynamic model (i.e. E-AIM (Clegg et al., 1998)):

$$k_{AC,i} = 10^{0.22pK_{BH_{i}} + 0.6X + 0.846R_{i} + log(a_{w}[H^{+}]) - 2.2}$$
(18)

The reactivity scale of lumping groups originated from the hydration equilibrium constant of various carbonyl compounds. Similar to $k_{AC,\ i}$, the oligomerization reaction rate constants in organic phase $(k_o, i, L \mod^{-1} \text{s}^{-1})$ are determined based on R_i and pK_{BH+i} without X and a_w $[H^+]$ terms:

$$k_{o,i} = 10^{0.22pK_{BH+i} + 0.846R_i - 3.9} (19)$$

4. Results and discussions

4.1. UNIPAR-GWP simulation vs. chamber observation

In order to examine the feasibility of the UNIPAR-GWP model, the predicted SOA mass was compared to the SOA data obtained from the photooxidation of toluene, TMB, and α -pinene under varying seed conditions and NO $_x$ levels (Table 1). Fig. 2 illustrates the time profiles of the

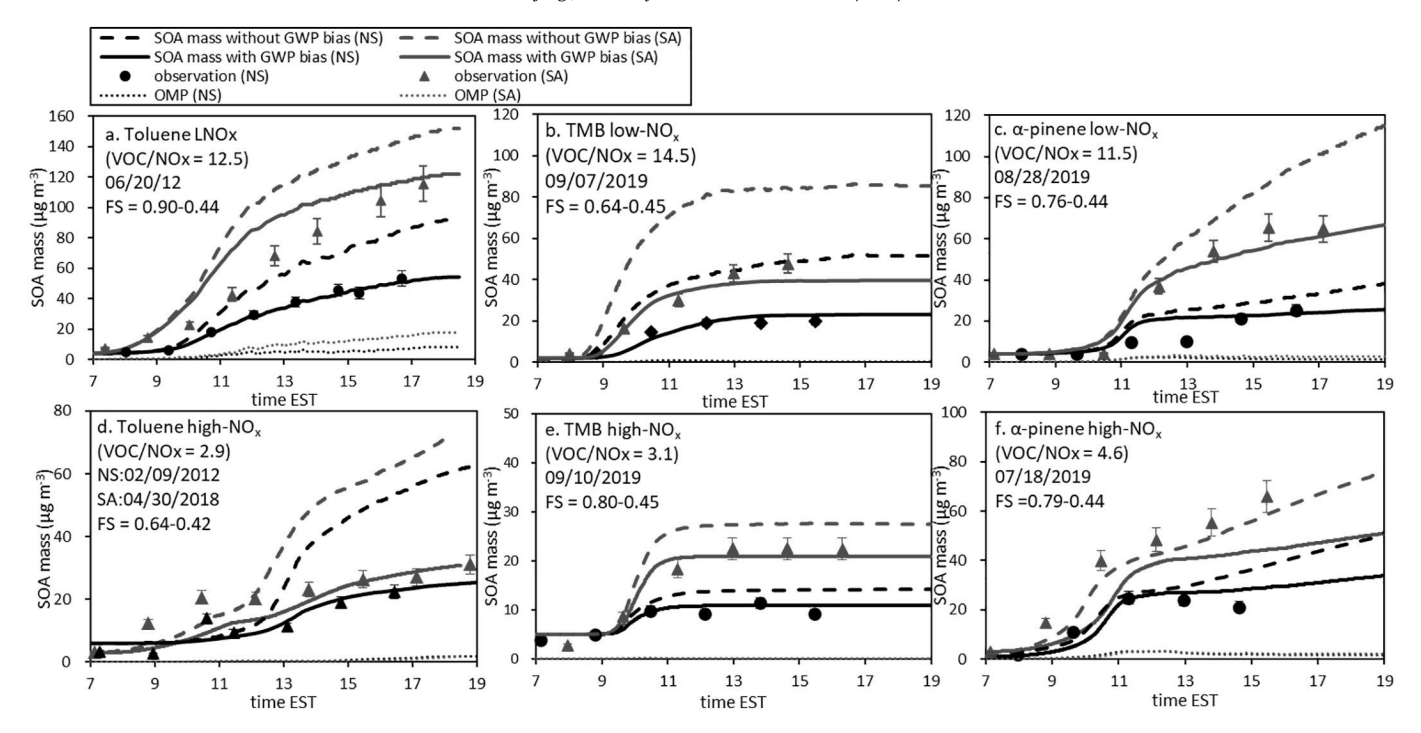


Fig. 2. Simulated SOA mass under the various experimental condition. The GWP impacted SOA mass (solid line) is presented with experimental observation (plot). The GWP corrected SOA mass (dashed line) and OM_P (dotted line) are predicted by simulating with updated SOA model parameter. The bias of experimental data due to the particle loss in the chamber was corrected. The error associated with SOA data is 9% according to the OC/EC analyzer and the collection of particle loss to the wall.

predicted SOA mass and the chamber observation for selected SOA systems (no seed and sulfuric acid-seed SOA). The simulation employs measured sunlight, temperature, and humidity during the chamber experiment. Supplementary Fig. S4 in Section S2 also demonstrates predictability of the UNIPAR-GWP model for the SOA data with SO₂ and those with wAS seed aerosol.

Overall, the predicted SOA mass reasonably demonstrates the impact of NO_x levels on SOA formation, yielding higher SOA mass under lower NO_x levels for all three HCs. Regardless of seed conditions, HC types and NO_x levels, SOA formation is dominated by OM_{AR} ($OM_{AR} = OM_T - OM_P$) as seen in Fig. 2. In the presence wet-inorganic aerosol, SOA formation increases due to oligomerization of the reactive organic compound dissolved in the aqueous phase. Additionally, SOA formation is significantly accelerated by an acid-catalyst in the presence of sulfuric acid aerosol as seen in Fig. 2. The impact of acidic seed on SOA growth in Fig. 2d was relatively small because humidity was lower than efflorescence RH (ERH) of partially neutralized sulfuric acid aerosol during the daytime. When RH drops below ERH, the UNIPAR model produces SOA mass only in organic phase.

Fig. 2 also illustrates the simulated SOA mass produced without the GWP artifact (dashed line) by using the UNIPAR-GWP model. In general, the reactivity of multifunctional organic compounds is poorly known. In UNIPAR-GWP, $k_{o,i}$ associated with the oligomerization of organic species in organic phase increased with a raised intercept to compensate the bias in SOA mass due to GWP of organic species. $k_{AC,i}$ for oligomerization in inorganic phase was also slightly increased with a raised intercept. k_{ACi} in Eq. (18) and k_{oi} in Eq. (19) are updated rate constants and they are applied to predict in-particle chemistry in UNIPAR-GWP. The impact of GWP on SOA formation varied depending upon the type of HCs, NO_x levels, and inorganic seed conditions. For example, aromatic SOA was generally more sensitive to the GWP bias than α -pinene SOA. This trend can be explained by the relative significance of the GWP time scales compared to the time scales for the aerosol formation originating from different product distributions in each HC. The characteristic timescale of important processes (i.e., GWP, gas-particle partitioning, oligomerization in the organic phase, aqueous reactions

in the inorganic phase) of various oxygenated products is discussed in Section 4.2 and applied to SOA sensitivity to important variables in Section 4.3.

4.2. Time scale of atmospheric processes of SVOCs

SOA growth can be affected by GWP when the timescale related to gas-particle equilibrium and aerosol phase reactions is competitive with that of GWP. Table S3 in Section S3.1 summarizes the characteristic time of GWP ($\tau_{GWP,i}$), gas-particle partitioning ($\tau_{GP,i}$), oligomerization in the organic phase $(\tau_{or,i})$ and aqueous reactions $(\tau_{in,i})$. Fig. 3 illustrates $au_{GWP,i}$, $au_{or,i}$, and $au_{in,i}$ of the selected oxidized product in each lumping group (Fig. S5 in Section S3.2 of Supplementary) for three HCs. $\tau_{GWP,i}$ ranges from 3 min to several hours. In general, $\tau_{GWP,i}$ increases with decreasing vapor pressure and increasing reactivity (generally, the more highly reactive *i* is the more polar). $\tau_{GP,i}$ is known to be a rapid process which can be done within several seconds. For example, Julin et al. reported τ_{GPi} can be as short as an order of 10^{-10} s (Julin et al., 2014). Thus, $\tau_{GP,i}$ is much shorter than $\tau_{GWP,i}$ and even smaller than aerosol phase reactions. $\tau_{or,i}$ varies with reactivity scales of i, ranging from 10^{-2} to 10^{10} s. The oligomerization can be accelerated by an acid catalyst in the aqueous phase. Thus, $au_{in,i}$ is shorter than $au_{or,i}$ as seen in Fig. 3. In general, 1VF-8VF, 1F—7F, and 1M-5M groups mainly contribute to SOA mass (OM_{AR}) because SOA formation is dominated by aerosol phase reactions of these reactive organic species. For those reactive groups, both $\tau_{in,i}$ and $\tau_{or,i}$ are much shorter than $\tau_{GWP,i}$ as seen in Fig. 3. Despite a considerable GWP process in group S, the impact of GWP is trivial due to a small contribution from the S group (weakly reactive) to SOA formation. Group P (partitioning only) is mainly influenced by GWP.

For the three SOA systems under the high-NO $_{\rm x}$ condition (HC/NO $_{\rm x}$ = 3 ppbC/ppb), major products related to SOA mass, GWP, and the total product concentration are marked in Fig. 3 to characterize the potential impact of GWP on SOA mass. For each SOA system, a black rectangular box represents major lumping species in non-seed (NS) SOA. In the presence of wet-ammonium hydrogen sulfate (wAHS), the lumping species that are

(Unit: s)															nit: s)													
	Tol									TMB									AP									
$ au_{GWP,i}$		1	2	3	4	5	6	7	8		1	2	3	4	5	6	7	8		1	2	3	4	5	6	7	8	
	VF	2E+05	1E+05	2E+05	2E+04	2E+04	6E+04	3E+04	2E+03	VF									VF	5E+05		1E+05	1E+06	6E+04	4E+04	6E+03	2E+03	
	F				8E+04	7E+04		1E+04	6E+02	F		7E+05	3E+05			3E+04	2E+04	2E+03	F				3E+04		2E+04	2E+04	4E+02	
	M	3E+05		* 6E+03	2E+04					M				3E+04			*1E+03		M		4E+04	1E+05	2E+05	4E+04	8E+04	* 4E+03	3E+02	
	S		9E+04		2E+04		**			S		1E+05	1E+05	8E+04	#			2E+03	S	8E+04	5E+04	1E+05	3E+05		# 8E+03	8E+03	3E+03	
	P	4E+05	5E+05	# 1E+03	6E+04	* 7E+02	2E+03	8E+02	3E+02	Р	7E+05	1E+05	9E+04	#8E+03	3E+03	# 4E+03	*2E+03		P		1E+04	1E+04	1E+04	* 2E+04	6E+03		7E+01	
	MA	1E+06								MA									MA		6E+04							
	R							2E+03	4E+02	R							2E+03	4E+02	R							2E+03	4E+02	
$ au_{{ m or},i}$			2	2	4	-	-	7	0		i a		_			-	-				•			-		-	•	
	VF	1 45.00	2	3		5	6	7 01	8		1	2	3	4	5	6	7	8	VF	1 15.00	2	3	4	5	6 1E-02	7	8	
	F	1E-02	1E-02	1E-02	1E-02 8E-01	1E-02 8E+00	1E-02	3E-01 8E+02	3E+00 8E+03	VF F		1E-02	9E-02			8E+01	8E+02	8E+03	F	1E-02		1E-02	1E-02 8E-01	1E-02		3E-01 8E+02	3E+00	
	M	6E+01		5E+02	5E+03	5E+04	5E+05	5E+06	5E+07	M		16-02	9E-02	5E+03	5E+04	9E+01	5E+02	5E+03			1E+02	5E+02	5E+03	5E+04	8E+01 5E+05	8E+02 5E+06	8E+03 5E+07	
	S	05+01	5E+04	2E+05	2E+06	2E+07	2E+08	2E+09	2E+10	S	_	5E+04	2E+05	2E+06	The second second	2E+08	2E+09	2E+10	M S	3E+04	5E+04	2E+05	2E+06	2E+07	2E+08	2E+09	2E+10	
	D	\vdash	JETU4	20703	2E+U0	25707	20700	20709	20+10	D D		JETU4	ZETUJ	ZETUU	ZETUI	ZETUO	25703	25710	P	3E+U4	3E+U4	20+05	2E+U0	20+07	20+00	20+09	20+10	
	MA	7E+01							$\overline{}$	MA									MA		1E+02							
	R	71.701						6E+02	1E+02	R							2E+00	3E+00	R		ILTUZ					2E+00	3E+00	
	00002 1002								1.00							88.50	00.00	"							21.00	32.00		
		1	2	3	4	5	6	7	8		1	2	3	4	5	6	7	8		1	2	3	4	5	6	7	8	
$ au_{\mathrm{in},i}$	VF	1E-02	1E-02	1E-02	1E-02	1E-02	1E-02	1E-02	1E-02	VF									VF	1E-02		1E-02	1E-02	1E-02	3E-01	1E-02	1E-02	
	F				1E-02	1E-02		3E+01	2E+03	F		1E-02	1E-02			4E+02	1E+01	3E+03	F				3E+00		2E+01	3E+01	2E+02	
	M	1E-02		1E+01	9E+02	3E+02	1E+04	6E+05	3E+08	M				2E+01	9E+03		1E+08	9E+04	M		2E+01	2E+02	1E+04	2E+05	1E+06	9E+07	4E+05	
	S		2E+03	3E+03	3E+04	5E+06	5E+06	5E+06	3E+08	S		8E+02	2E+04	3E+06	5E+06	1E+07	1E+08	3E+09	S	9E+01	3E+03	5E+05	4E+06	1E+08	1E+09	2E+09	3E+08	
	P									P									P									
	MA	2E-01								MA									MA		2E+00							
	R							2E+01	1E-02	R							6E-02	1E-02	R							6E-02	1E-02	

Fig. 3. The characteristic timescale (s) based on the lumping group of UNIPAR. The estimated characteristic timescale is calculated based on the selected oxidized products in Fig. S4 in Supplementary. The major groups generating SOA under high NO_x condition (HC/ NO_x = 3 ppbC/ppb) in the organic phase are marked with black border and additional compounds contributing SOA formation in the presence of wAHS by the aqueous phase reaction with acid catalyst are marked with red border. The major groups contributing to total product concentrations (gas+aerosol+wall) and to wall are marked with * in red color and * in blue color in lumping bins, respectively.

additionally involved in SOA formation via acid-catalyzed reactions, are marked with a red rectangular box. In each SOA, the lumping groups that have a large total concentration (gas+particle+wall) are marked as symbol * in red color. These lumping groups may possibly contribute to GWP. Symbol # in blue color represents the group that can significantly contribute to GWP. Overall, the GWP dominant groups are not overlapped with SOA major contributors. The GWP contributors of α -pinene products are relatively more volatile than those in toluene or TMB. GWP dominant lumping species (symbols * and #) are volatile or mainly in S and P groups, except group 3M in toluene.

4.3. Sensitivity of SOA formation to major variables in the absence of GWP bias

In order to characterize the sensitivity of SOA formation to major environmental variables, the formation of SOA is simulated for the photo-oxidation of 30 ppb HCs (toluene, TMB, and α -pinene) under two NO_x levels (HC ppbC/NO_x ppb = 3 and 12), two humidity levels (45% and 80%), two temperature (278 K and 298 K) and three seed conditions (NS, wAS (neutral seed), wAHS (acidic seed)) using the sunlight profile on 6/19/2015 (Fig. S6 in Section S4). In order to simulate the SOA formation under the urban environmental condition, pre-existing organic matter (OM_0) is set to 5 $\mu g \ m^{-3}$ the inorganic seed concentration (wAS and wAHS) was set to 20 $\mu g \ m^{-3}$. Fig. 4 illustrates simulated SOA mass after a 12 h reaction (I, III, V) under various environmental conditions in the absence and presence of GWP artifacts. In Fig. 4 SOA mass is plotted to HC consumption (II, IV, and VI) with and without GWP bias.

A noticeable change appeared between NS SOA and wAS seeded SOA suggesting that SOA growth changes at the efflorescence RH for all three HC, especially for toluene. The impact of RH on SOA formation at the high temperature (298 K) is, however, less than the phase transition of inorganic seed if RH is higher than ERH for the SOA aerosol processed under the liquid-liquid phase separation (LLPS) mode between the organic phase and the inorganic phase. SOA growth for the three HCs of this study is simulated with LLPS and shows insignificant RH impact

on SOA mass (i.e., Fig. 4 E, F vs. G, H). A similar result appeared in the recent study by Zhou et al. (2019) for three monoalkylbenzene SOAs (toluene, ethylbenzene, and n-propylbenzene) at 298 K. The model simulation is in accordance with the typical trend (Hallquist et al., 2009; Ng et al., 2007) in NO_x effect on SOA mass showing the higher SOA mass with the lower NO_x level (i.e., Fig. 4 A, C, E, G vs. B, D, F, H) for all three HCs. The α -pinene SOA was somewhat less sensitive to NO_x levels than aromatic SOAs. The model also captures the impact of temperature on SOA formation, where partitioning mass increased at lower temperatures. Evidently, the UNIPAR simulation concurred with chamber-generated SOA data collected in different seasons (different temperatures) as seen in Fig. 2 and Table 1. The SOA mass drastically increase by factors of 2 to 4 with decreasing temperature from 298 and 278 K (Fig. 4 E-H vs. A-D). The temperature is the most influential factor on SOA mass within our sensitivity evaluation. The sensitivity to temperature is the highest with TMB and the least with toluene.

The simulation of SOA formation is performed for three different seed conditions: NS, wAS, and wAHS, in the absence and the presence of GWP. The seed effects on SOA formation were dependent on HC types. For example, toluene SOA (Fig. 4-II) significantly increases with both wAS and wAHS (more than doubling SOA yields at given simulation conditions with wall). For TMB and α -pinene (Fig. 4-IV and 4-VI), a significant increase in SOA yields appeared with wAHS-seeded acidic aerosol. This different trend in inorganic seed impacts on SOA between toluene and other two HCs can be explained by $\gamma_{in,i}$ (solubility in aqueous phase) of oxidized products as described in Section S5 in Supplementary. Fig. S7 illustrates $\gamma_{in,i}$ of oxidized products in three SOA systems (see Eq. (15) in Section 3.2). The $\gamma_{in,i}$ values of oxidized products in TMB and α -pinene are generally larger than those in toluene, resulting in low solubility in the aqueous phase. Without an acidcatalyst, SOA growth, therefore, inorganic seed effect is less in TMB and α -pinene than toluene.

The top portion in the stack bar in I, III, and V series of Fig. 4 illustrate the impact of GWP on various SOA. Aromatic SOAs are more sensitive to GWP bias than α -pinene. For example, the SOA mass change in toluene ranges from 9 to 71% due to GWP, while that in α -pinene is relatively

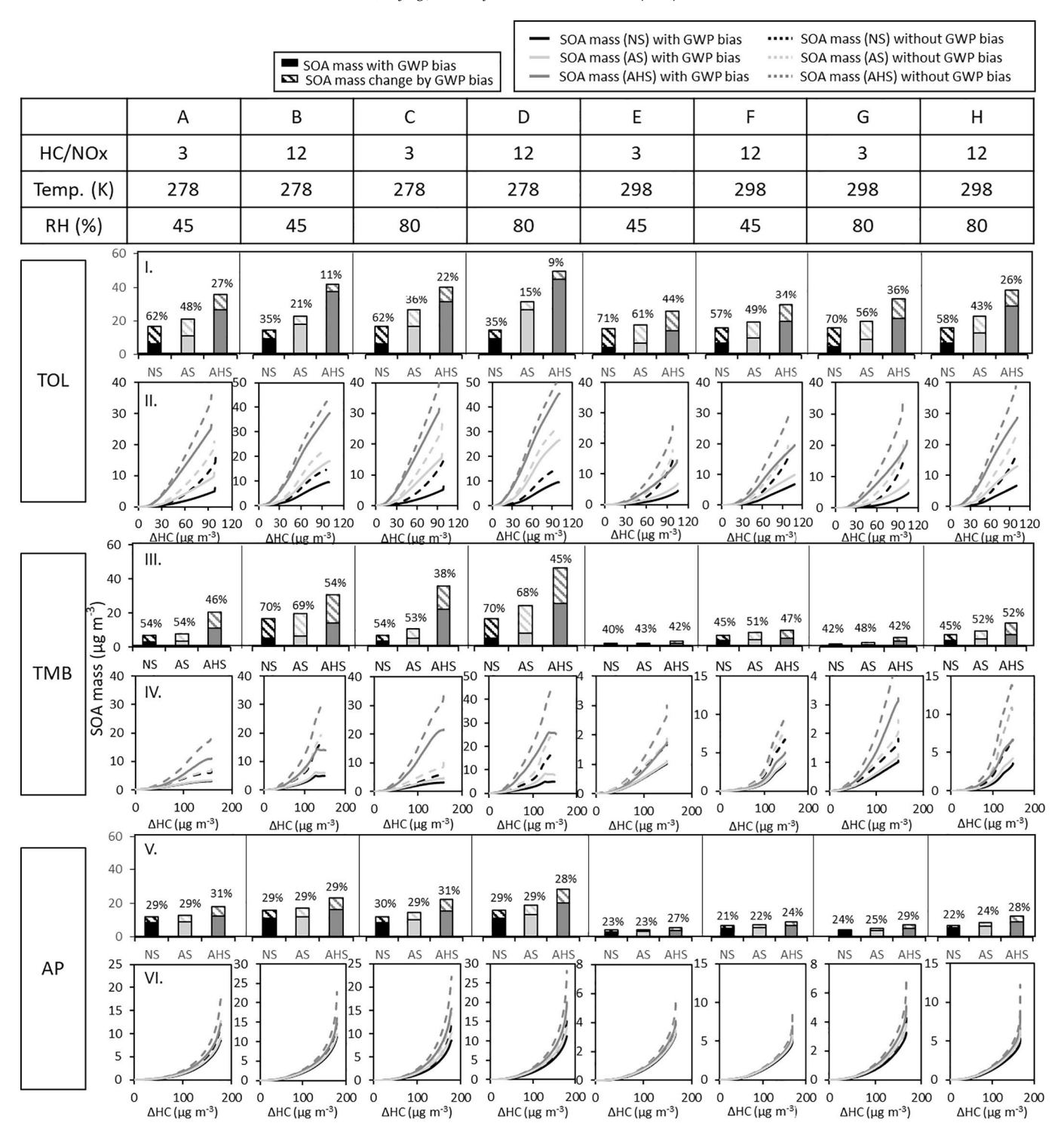


Fig. 4. The sensitivity of SOA formation to important variables (temperature, humidity, NO_x level, seed types) for three different HCs (toluene (TOL), 1,3,5-trimethylbenzene (TMB), and α -pinene (AP)). The simulation of SOA mass was performed for the photooxidation of hydrocarbons at a given experimental conditions under the ambient sunlight measured on 06/19/2015 (presented in Fig. S6). The initial concentration of HC was 30 ppb and OM_0 was set to 5 μ g m $^{-3}$. The inorganic seed concentration ((NH₄)₂SO₂ (AS) and NH₄HSO₂ (AHS)) was set to 20 μ g m $^{-3}$. Series I, III, and V represent the SOA mass produced after 12 h simulation. For series of I, III, and V, the percentage on each bar represents the decreased SOA mass by the impact of GWP compare to the SOA mass without a GWP bias. Series II, IV, and VI illustrate the SOA mass as a function of HC consumption in the presence and the absence of the GWP bias.

insensitive to temperature, RH, NO_x , and seed conditions (23–31%). For toluene SOA, the GWP fraction of total SOA in the absence of wet seed (NS) is significantly higher than that in the presence of wet seed (wAS or wAHS) regardless of NO_x levels. We can conclude that the GWP fraction of total SOA mass is relatively less significant for simulation of acidic-seeded SOA formation for all HCs except TMB at the high temperature (298 K).

The importance of GWP can also be different by the initial concentration of HC in the chamber experiment. Fig. 5 illustrates the SOA mass produced from the photooxidation of toluene or α -pinene at the three different initial HC concentrations (10, 30, and 60 ppb). The SOA mass drastically increased when the initial HC concentration increased because of the promotion of gas-particle partitioning with increasing OM_T (Odum et al., 1996). Consequently, increased partitioning mass

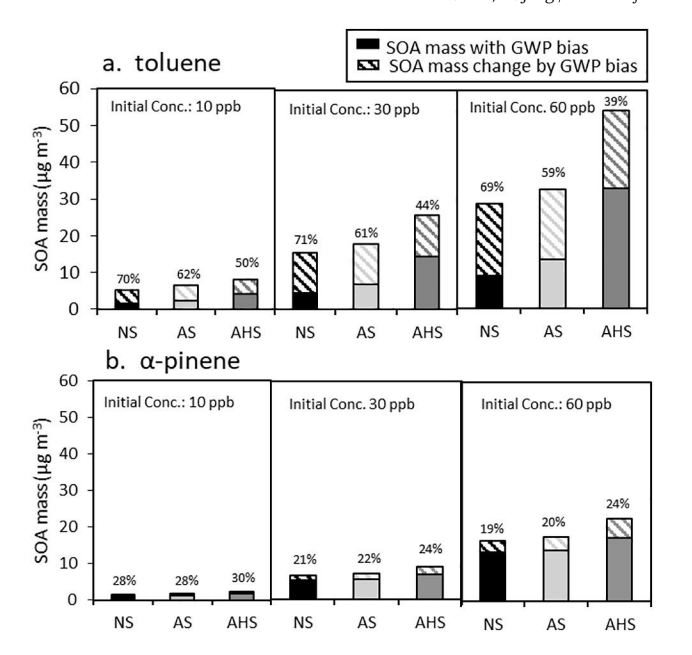


Fig. 5. The impact of GWP on SOA mass under varying the initial concentration of toluene and α-pinene at a given conditions (T=298 K, RH=45%) with the certain NO_x condition (toluene: high-NO_x, α-pinene: low-NO_x) under the ambient sunlight measured on 06/19/2015 (presented in Fig. S6). The inorganic seed concentration (AS and AHS) was set to 20 μg m⁻³. The percentage on each bar represents the decreased SOA mass by the impact of GWP compare to the SOA mass without a GWP bias.

accelerates aerosol phase reactions of organics. Overall, the GWP fraction of total SOA mass is, however, less with a higher initial HC concentration. It suggests that model parameters obtained from the low HC concentrations in past chamber studies might be more biased due to GWP.

4.4. Chamber characteristic parameters vs. GWP impacts on SOA prediction

The impact of GWP on SOA formation is also influenced by chamber dimensions and its surface properties. Fig. 6 demonstrates the sensitivity of SOA formation to chamber parameters, OM_{wall} and A/V, in the presence of GWP. The OM_{wall} of UF-APHOR is 18.52 mg m⁻³ and the A/V ratio is 1.65. The upper boundary of OM_{wall} is set to 40 mg m⁻³ and the lower boundary to 10 mg m⁻³. The upper boundary of the A/

V ratio is set to 3.3 (double of UF-APHOR) and the lower boundary to 1.2 (sphere with 2.5 m diameter). The SOA mass decreases by increasing OM_{wall} and/or the A/V ratio owing to GWP. $K_{w,i}$ increases with increasing OM_{wall} (Eq. (4)) and $k_on_{w,i}$ increases with A/V (Eq. (6)). Within our boundaries, the A/V ratio is more influential on SOA mass than OM_{wall} . The upper boundary of the A/V ratio (3.3) can closely represent the parameters of typical indoor chambers that are smaller than the UF-APHOR chamber. With the upper boundary of A/V ratio in Fig. 6, the reduction of $\tau_{GWP,i}$ of organic species are various raging from half to an order of magnitude compared to the reference (UF-APHOR). With lowering OM_{wall} , $\tau_{GWP,i}$ decreases by half. Thus, $\tau_{GWP,i}$ of organic compounds in the smaller indoor chamber possibly would be one order of magnitude shorter than that of a large outdoor chamber. The aromatic SOA is more sensitive to the chamber characteristic parameters than α -pinene.

4.5. Model uncertainties

Fig. 7 represents the uncertainties of the SOA prediction when changing major model parameters ($k_on_{w,i}$, $\gamma_{w,i}$, $p_{L,i}$, $k_{o,i}/k_{AC,i}$, and $\gamma_{in,i}$) in the presence of GWP. SOA mass is reduced by the raised $k_on_{w,i}$, which gears toward reduction of characteristic time. Furthermore, the change in chemical distribution due to GWP can alter gas chemistry and cause further changes in SOA production. In the partitioning point, the increased $\gamma_{w,i}$ should increase SOA mass but simulation shows the reduction in SOA mass suggesting that sequential reactions in gas phase can considerably influence product distributions.

 $p_{L,\,i}^*$ can influence both GWP (Eq. (4)) and gas-particle partitioning in UNIPAR (Eqs. (13) and (14)). Model parameter $\gamma_{in,\,i}$ (Eq. (15)) and aerosol phase rate constants (Eq. (18)) in inorganic phase are associated with the UNIPAR model. For the three HCs, the uncertainties of the SOA prediction in changing UNIPAR model parameters are varied because each HC will produce different SVOCs that have different solubility in the aqueous phase and reactivity in the aerosol phase. In the absence of GWP, the uncertainties of the SOA prediction in varying the model parameters associated with UNIPAR are shown in Fig. S8 (Section S6 in Supplementary), showing a similar tendency in Fig. 7.

5. Atmospheric implication

The simulation of this study showed that SOA formation was influenced by NO_x levels, RH, seed types, and temperature as shown in Section 4.3 and Fig. 4. Such trends in SOA formation were in accordance with previously reported studies (Hallquist et al., 2009). SOA production

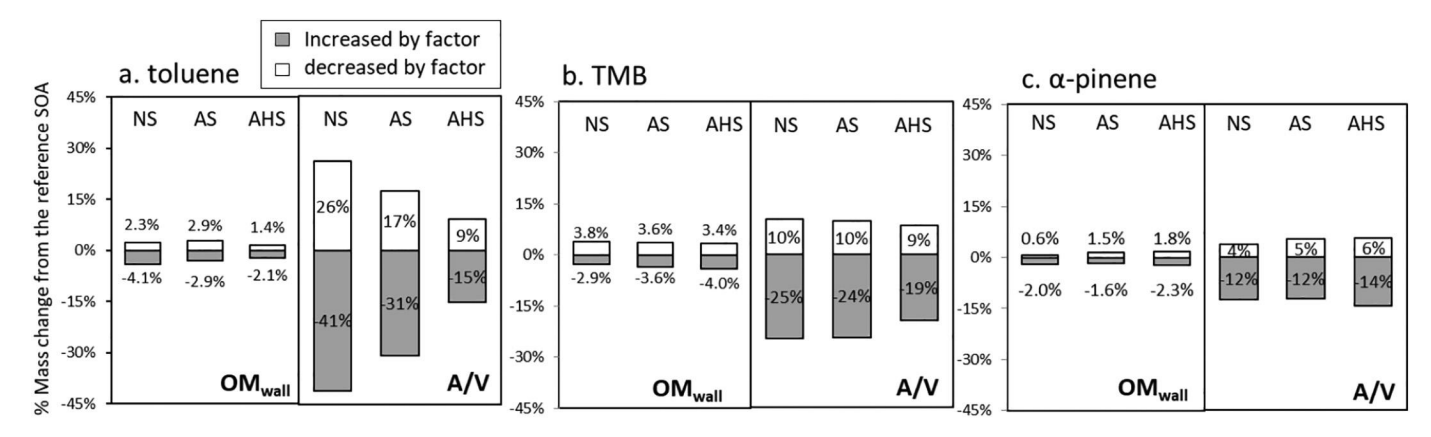


Fig. 6. The sensitivity of SOA mass to the chamber specific parameters is predicted by changing OM_{wall} and A/V ratios at a given conditions (T = 298 K, RH = 45%) under the certain NO_x condition (aromatic HCs: high- NO_x , α-pinene: low- NO_x). The SOA mass is simulated with 30 ppb of each hydrocarbon under the sunlight on 06/19/2015 measured in the UF-APHOR. The inorganic seed concentration wAS and wAHS) was set to $20 \, \mu g \, m^{-3}$. The reference condition is set to the chamber characteristic parameters of UF-APHOR ($OM_{wall} = 18.52 \, mg \, m^{-3}$ and A/V = 1.65). The upper boundary (filled) and lower boundary (open) of OM_{wall} are $40 \, mg \, m^{-3}$ and $10 \, mg \, m^{-3}$, respectively. The shape of UF-APHORE is semi-cylindric ($r = 2.5 \, m$) and its A/V ratio is 1.65. The upper boundary and the lower boundary of A/V ratio are 3.33 (double of the UF-APHOR) and 1.2 (sphere shape with $r = 2.5 \, m$), respectively.

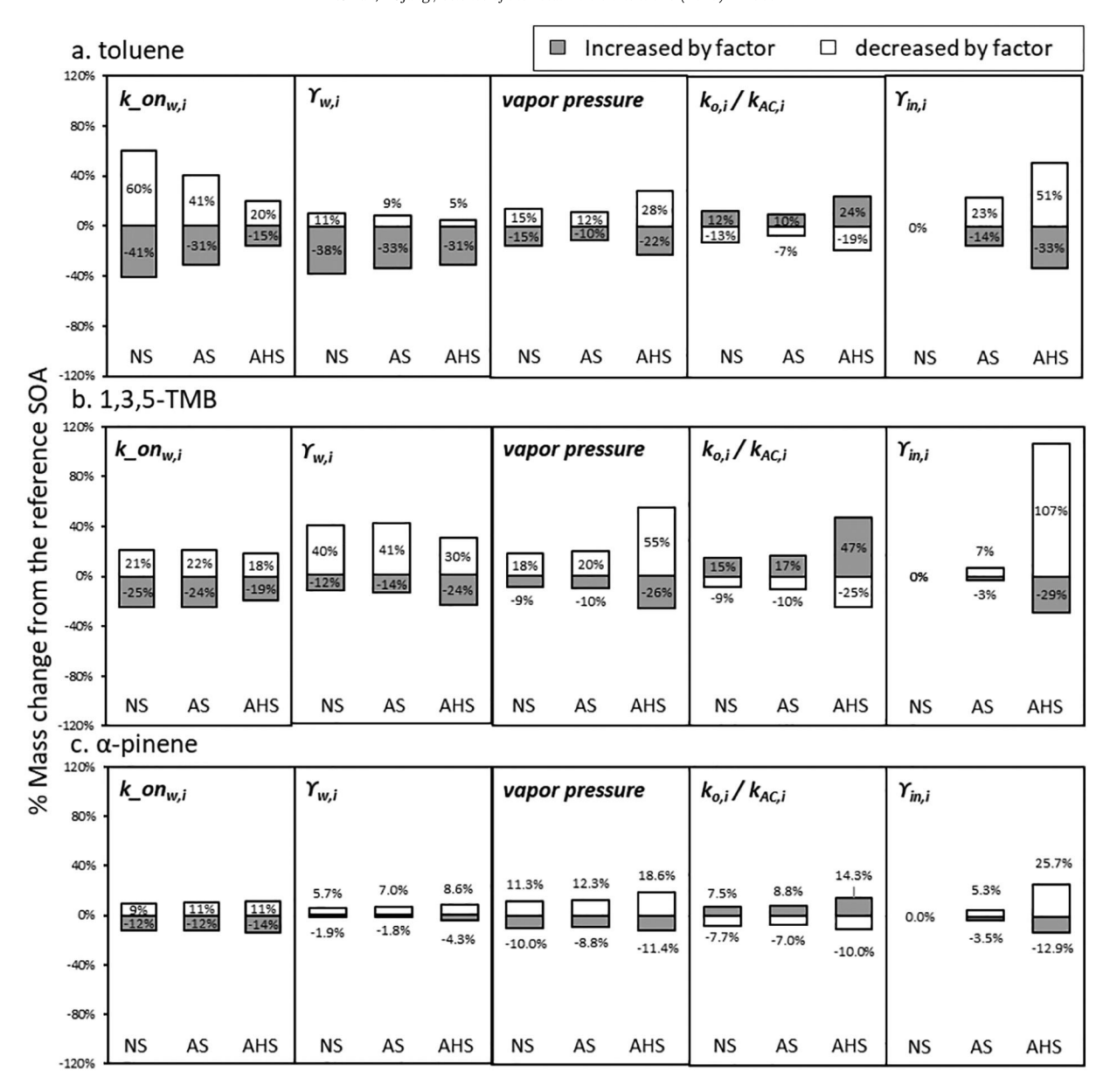


Fig. 7. The uncertainties in the prediction of SOA mass using the UNIPAR model in the presence of GWP by varying important model parameters $(k_on_{w,b}, \gamma_{w,b}, p_{\iota,i}^{\circ}, k_{o,j}/k_{AC,b}, and \gamma_{in,l})$ at a given conditions (T = 298 K, RH = 45%) under the certain NO_x level (aromatic HCs: high-NO_x, α-pinene: low-NO_x). The SOA mass is simulated with 30 ppb under the sunlight on 06/19/2015 measured in the UF-APHOR (Fig. S6). The inorganic seed concentration (AS and AHS) was set to 20 μg m⁻³. The variations in $k_on_{w,b}, \gamma_{w,b}, k_{o,j}/k_{AC,b}$ and $\gamma_{in,l}$ are 2 times and 0.5 times. The variations in vapor pressure are 1.5 times and 0.67 times.

was more sensitive to aerosol acidity (wAS vs. wAHS) than that to humidity (45% vs 80%). SOA mass increases in the presence of wet-seed but the sensitivity of SOA formation to RH is less when RH is higher than ERH. This was shown by a change in ERH due to the inorganic aerosol phase transition. Unlike the SOA in the LLPS mode, isoprene SOA is mixable with wet inorganic salts to form a single homogeneously mixed phase (Beardsley and Jang, 2016) and is sensitive to RH even after ERH. Thus, the aerosol phase mode can be a key to simulate the sensitivity of SOA formation to RH.

The explicit approach in the UNIPAR-GWP model benefits the prediction of GWP that has varied physicochemical properties of a variety of organic species as well as the simulation of aerosol phase reactions of various reactive oxygenated products. As seen in Section 4.3, the impact of GWP varies with HC types, NO_x , RH, temperature, and seed conditions. Although the partitioning theory can partially explain the trend in the impact of GWP on SOA formation, the prediction of SOA mass with GWP is complex due to nonlinearity in gas chemistry. In general,

aromatic HCs are more impacted by GWP than and α -pinene. GWP fraction of total SOA is greater with the lower consumption of HC in the absence of wet-inorganic seed (Fig. 5). When the GWP-biased model parameter is applied to SOA formation in SO₂ poor environments, the simulation can considerably underestimate SOA mass. Studies showed that SOA mass at regional or global scales was underestimated against observed values (Volkamer et al., 2006; Ensberg et al., 2014; Baker et al., 2015). In general, ambient SOA is produced in the presence of preexisting wet-inorganic seed (Ervens et al., 2011). As seen in this study, the GWP bias in SOA mass in the presence of inorganic seed is relatively small, suggesting that that GWP corrected model parameters can somewhat advance predictions but still insufficient to improve underestimation of SOA mass. Therefore, the formation of non-volatile oligomers via aqueous reactions of organic species in the presence of electrolytic inorganic aerosols might be important mechanisms to identify the missing source of SOA. In the regional models, aqueous reactions of a variety of organic species orienting from numerous HCs are still

missing (McDonald et al., 2018). The model simulation of this study also proves the importance of aqueous reactions, as it shows an increase in SOA mass in the presence of wet-inorganic aerosol compared to that in the absence of seed (Fig. 4).

The UNIPAR-GWP model of this study can be applied to SOA data originating from other laboratories, if the chamber characteristic parameters are substituted (OM_{wall} and A/V, Eqs. (4) and (6)). The outdoor chamber of this study is exposed to ambient air during the ventilation process after each experiment and the chamber air is flushed using clean air for at least two days under natural sunlight. However, the cleaning procedure of the chamber in other laboratories may be different from the outdoor chamber: i.e., cleaning using tank air after each experiment without contact with ambient air. Thus, OMwall and its compositions may be different between chambers. Then, the coefficients in the QSAR-base polynomial equation (Eqs. (7) and (8)) should be recalculated to apply the GWP model of this study to different chambers. Furthermore, the alteration of SOA production by GWP is nonlinear to chamber dimension due to sequential gas chemistry. The SOA model parameters previously employed in regional models were determined by using chamber studies conducted in indoor chambers with high A/V ratios (2.0–3.0) (see Section 4.4). The data originating from smaller chambers might lead more bias due to the greater GWP associated with the larger k_ $on_{w,i}$.

Although not investigated in detail in this study, the aerosol viscosity may play an important role in SOA formation in low O:C ratios (Shiraiwa et al., 2011). For example, Renbaum-Wolff et al. reported a slow diffusion of α -pinene SOA due to its high viscosity (Renbaum-Wolff et al., 2013), as this affected the bulk diffusivity in the aerosol (Koop et al., 2011). The limited diffusion in the aerosol phase can inhibit gas particle partitioning, as well as aerosol phase reactions. In addition, the UNIPAR-GWP model employed MCM (Jenkin et al., 2012). MCM can cause the uncertainty of GWP bias, as well as the prediction of SOA. Crounse et al. discovered that autooxidation in terpene systems can produce nonvolatile multifunctional alcohols and increases SOA mass (Bianchi et al., 2019; Crounse et al., 2013). The autooxidation mechanism was not considered in this study.

The various functionalities of SVOCs were applied to establish the QSAR based GWP model. More accurate data allowed for the better QSAR based GWP model. The QSAR model was demonstrated mostly with mono-functional organic species. Many organic species in SOA are multifunctional but they are not commercially available. In addition, the measurement of initial gas-phase concentration is burdensome because the experimental procedure requires the time step for the vaporization of organic species into a chamber. In order to improve the robustness of the GWP model, the database should be extended to multifunctional organics with a short chemical injection method and continuous online detection of gaseous compounds.

CRediT authorship contribution statement

Sanghee Han: Formal analysis, Writing - original draft, Visualization. **Myoseon Jang:** Methodology, Conceptualization, Writing - review & editing, Supervision.

Declaration of competing interest

The authors declare that they have no known competing financial interests or personal relationships that could have appeared to influence the work reported in this paper.

Acknowledgment

This research was supported by the awards from the NSF (AGS 1923651) and the National Strategic Project-Fine particle of the National Research Foundation of Korea (NRF) funded by the Ministry of

Science and ICT (MSIT), the Ministry of Environment (ME), and the Ministry of Health and Welfare (MOHW) (2017M3D8A1090654).

Appendix A. Supplementary data

Supplementary data to this article can be found online at https://doi. org/10.1016/j.scitotenv.2020.141360.

References

- Abraham, M., McGowan, J., 1987. The use of characteristic volumes to measure cavity terms in reversed phase liquid-chromatography. Chromatographia 23, 243–246. https://doi.org/10.1007/BF02311772.
- Abraham, M., Whiting, G., Doherty, R., Shuely, W., 1991. Hydrogen-bonding. 16. A new solute solvation parameter, Pi-2(H), from gas-chromatographic data. J. Chromatogr. 587, 213–228. https://doi.org/10.1016/0021-9673(91)85158-C.
- Alan, R., 1992. Model solvent systems for QSAR. Part 3. An LSER analysis of the 'critical quartet.' New light on hydrogen bond strength and directionality. J. Chem. Soc. Perkin Trans. 2, 705–722.
- Appel, K.W., Napelenok, S.L., Foley, K.M., Pye, H.O., Hogrefe, C., Luecken, D.J., Bash, J.O., Roselle, S.J., Pleim, J.E., Foroutan, H., 2017. Description and evaluation of the Community Multiscale Air Quality (CMAQ) modeling system version 5.1. Geosci. Model Dev. 10. 1703.
- Arp, H., Goss, K., 2009. Ambient gas/particle partitioning. 3. Estimating partition coefficients of apolar, polar, and ionizable organic compounds by their molecular structure. Environ. Sci. Technol. 43, 1923–1929. https://doi.org/10.1021/es8025165.
- Baker, K., Carlton, A., Kleindienst, T., Offenberg, J., Beaver, M., Gentner, D., Goldstein, A., Hayes, P., Jimenez, J., Gilman, J., 2015. Gas and aerosol carbon in California: comparison of measurements and model predictions in Pasadena and Bakersfield. Atmos. Chem. Phys. 15, 5243–5258.
- Barsanti, K., Carlton, A., Chung, S., 2013. Analyzing experimental data and model parameters: implications for predictions of SOA using chemical transport models. Atmos. Chem. Phys. 13, 12073–12088. https://doi.org/10.5194/acp-13-12073-2013.
- Barsanti, K.C., Kroll, J.H., Thornton, J.A., 2017. Formation of low-volatility organic compounds in the atmosphere: recent advancements and insights. J. Phys. Chem. Lett. 8, 1503–1511.
- Barton, A.F., 2017. CRC Handbook of Solubility Parameters and Other Cohesion Parameters. Routledge.
- Beardsley, R., Jang, M., 2016. Simulating the SOA formation of isoprene from partitioning and aerosol phase reactions in the presence of inorganics. Atmos. Chem. Phys. 16, 5993–6009. https://doi.org/10.5194/acp-16-5993-2016.
- Bi, X., Sheng, G., Peng, P.A., Chen, Y., Zhang, Z., Fu, J., 2003. Distribution of particulate-and vapor-phase n-alkanes and polycyclic aromatic hydrocarbons in urban atmosphere of Guangzhou, China. Atmos. Environ. 37, 289–298.
- Bianchi, F., Kurten, T., Riva, M., Mohr, C., Rissanen, M., Roldin, P., Berndt, T., Crounse, J., Wennberg, P., Mentel, T., Wildt, J., Junninen, H., Jokinen, T., Kulmala, M., Worsnop, D., Thornton, J., Donahue, N., Kjaergaard, H., Ehn, M., 2019. Highly oxygenated organic molecules (HOM) from gas-phase autoxidation involving peroxy radicals: a key contributor to atmospheric aerosol. Chem. Rev. 119, 3472–3509. https://doi.org/10.1021/acs.chemrev.8b00395.
- Bowman, F.M., Odum, J.R., Seinfeld, J.H., Pandis, S.N., 1997. Mathematical model for gasparticle partitioning of secondary organic aerosols. Atmos. Environ. 31, 3921–3931.
- Cappa, C.D., Jathar, S.H., Kleeman, M.J., Docherty, K.S., Jimenez, J.L., Seinfeld, J.H., Wexler, A.S., 2016. Simulating secondary organic aerosol in a regional air quality model using the statistical oxidation model–part 2: assessing the influence of vapor wall losses. Atmos. Chem. Phys. 16.
- Carlton, A.G., Wiedinmyer, C., Kroll, J.H., 2009. A review of secondary organic aerosol (SOA) formation from isoprene. Atmos. Chem. Phys. 9, 4987–5005.
- Clegg, S.L., Brimblecombe, P., Wexler, A.S., 1998. Thermodynamic model of the system H + NH4+ S042 N03 H2O at tropospheric temperatures. J. Phys. Chem. A 102, 2137–2154.
- Cohen, A., Brauer, M., Burnett, R., Anderson, H., Frostad, J., Estep, K., Balakrishnan, K., Brunekreef, B., Dandona, L., Dandona, R., Feigin, V., Freedman, G., Hubbell, B., Jobling, A., Kan, H., Knibbs, L., Liu, Y., Martin, R., Morawska, L., Pope, C., Shin, H., Straif, K., Shaddick, G., Thomas, M., van Dingenen, R., van Donkelaar, A., Vos, T., Murray, C., Forouzanfar, M., 2017. Estimates and 25-year trends of the global burden of disease attributable to ambient air pollution: an analysis of data from the Global Burden of Diseases Study 2015. Lancet 389, 1907–1918. https://doi.org/10.1016/S0140-6736(17)30505-6.
- Crounse, J.D., Nielsen, L.B., Jørgensen, S., Kjaergaard, H.G., Wennberg, P.O., 2013. Autoxidation of organic compounds in the atmosphere. The Journal of Physical Chemistry Letters 4, 3513–3520.
- Donahue, N., Robinson, A., Stanier, C., Pandis, S., 2006. Coupled partitioning, dilution, and chemical aging of semivolatile organics. Environ. Sci. Technol. 40, 2635–2643. https://doi.org/10.1021/es052297c.
- Endo, S., Goss, K., 2014. Applications of Polyparameter linear free energy relationships in environmental chemistry. Environ. Sci. Technol. 48, 12477–12491. https://doi.org/ 10.1021/es503369t.
- Ensberg, J., Hayes, P., Jimenez, J., Gilman, J., Kuster, W., De Gouw, J., Holloway, J., Gordon, T., Jathar, S., Robinson, A., 2014. Emission factor ratios, SOA mass yields, and the impact of vehicular emissions on SOA formation. Atmos. Chem. Phys. 14, 2383–2387.

- Ervens, B., Turpin, B., Weber, R., 2011. Secondary organic aerosol formation in cloud droplets and aqueous particles (aqSOA): a review of laboratory, field and model studies. Atmos. Chem. Phys. 11, 11069–11102.
- Gundel, L., Lee, V., Mahanama, K., Stevens, R., Daisey, J., 1995. Direct determination of the phase distributions of semivolatile polycyclic atomatic-hydrocarbons using annular denuders. Atmos. Environ. 29, 1719–1733. https://doi.org/10.1016/1352-2310(94) 00366-S.
- Hallquist, M., Wenger, J., Baltensperger, U., Rudich, Y., Simpson, D., Claeys, M., Dommen, J., Donahue, N., George, C., Goldstein, A., Hamilton, J., Herrmann, H., Hoffmann, T., linuma, Y., Jang, M., Jenkin, M., Jimenez, J., Kiendler-Scharr, A., Maenhaut, W., McFiggans, G., Mentel, T., Monod, A., Prevot, A., Seinfeld, J., Surratt, J., Szmigielski, R., Wildt, J., 2009. The formation, properties and impact of secondary organic aerosol: current and emerging issues. Atmos. Chem. Phys. 9, 5155–5236. https://doi.org/10.5194/acp-9-5155-2009.
- Han, S., Jang, M., and Jiang, H.: Modeling of gas-wall partitioning of organic compounds using a quantitative structure-activity relationship, Atmos. Chem. Phys. Discuss., https://doi.org/https://doi.org/10.5194/acp-2019-550, 2019.
- Huang, Y., Zhao, R., Charan, S., Kenseth, C., Zhang, X., Seinfeld, J., 2018. Unified theory of vapor-wall mass transport in teflon-walled environmental chambers. Environ. Sci. Technol. 52, 2134–2142. https://doi.org/10.1021/acs.est.7b05575.
- Im, Y., Jang, M., Beardsley, R., 2014. Simulation of aromatic SOA formation using the lumping model integrated with explicit gas-phase kinetic mechanisms and aerosolphase reactions. Atmos. Chem. Phys. 14.
- Jang, M., Kamens, R.M., 1999. A predictive model for adsorptive gas partitioning of SOCs on fine atmospheric inorganic dust particles. Environ. Sci. Technol. 33, 1825–1831.
- Jang, M., Czoschke, N., Lee, S., Kamens, R., 2002. Heterogeneous atmospheric aerosol production by acid-catalyzed particle-phase reactions. Science 298, 814–817. https://doi.org/10.1126/science.1075798.
- Jang, M., Czoschke, N.M., Northcross, A.L., 2005. Semiempirical model for organic aerosol growth by acid-catalyzed heterogeneous reactions of organic carbonyls. Environ. Sci. Technol. 39, 164–174.
- Jang, M., Sun, S., Winslow, R., Han, S., Yu, Z., 2020. In situ aerosol acidity measurements using a UV–Visible micro-spectrometer and its application to the ambient air. Aerosol Sci. Technol. 54, 446–461.
- Jenkin, M., Wyche, K., Evans, C., Carr, T., Monks, P., Alfarra, M., Barley, M., McFiggans, G., Young, J., Rickard, A., 2012. Development and chamber evaluation of the MCM v3.2 degradation scheme for beta-caryophyllene. Atmos. Chem. Phys. 12, 5275–5308. https://doi.org/10.5194/acp-12-5275-2012.
- Julin, J., Winkler, P.M., Donahue, N.M., Wagner, P.E., Riipinen, I., 2014. Near-unity mass accommodation coefficient of organic molecules of varying structure. Environ. Sci. Technol. 48, 12083–12089.
- Koop, T., Bookhold, J., Shiraiwa, M., Pöschl, U., 2011. Glass transition and phase state of organic compounds: dependency on molecular properties and implications for secondary organic aerosols in the atmosphere. Phys. Chem. Chem. Phys. 13, 19238–19255.
- Krechmer, J., Pagonis, D., Ziemann, P., Jimenez, J., 2016. Quantification of gas-wall partitioning in teflon environmental chambers using rapid bursts of low-volatility oxidized species generated in situ. Environ. Sci. Technol. 50, 5757–5765. https://doi.org/ 10.1021/acs.est.6b00606.
- La, Y., Camredon, M., Ziemann, P., Valorso, R., Matsunaga, A., Lannuque, V., Lee-Taylor, J., Hodzic, A., Madronich, S., Aumont, B., 2016. Impact of chamber wall loss of gaseous organic compounds on secondary organic aerosol formation: explicit modeling of SOA formation from alkane and alkene oxidation. Atmos. Chem. Phys. 16, 1417–1431. https://doi.org/10.5194/acp-16-1417-2016.
- Leach, K., Kamens, R., Strommen, M., Jang, M., 1999. Partitioning of semivolatile organic compounds in the presence of a secondary organic aerosol in a controlled atmosphere. J. Atmos. Chem. 33, 241–264. https://doi.org/10.1023/A:1006108430033.
- Li, J., Jang, M., Beardsley, R.L., 2016. Dialkylsulfate formation in sulfuric acid-seeded secondary organic aerosol produced using an outdoor chamber under natural sunlight. Environ. Chem. 13, 590–601.
- Lyu, R., Shi, Z., Alam, M.S., Wu, X., Liu, D., Vu, T.V., Stark, C., Xu, R., Fu, P., Feng, Y., 2019. Alkanes and aliphatic carbonyl compounds in wintertime PM2. 5 in Beijing, China. Atmos. Environ. 202, 244–255.
- Matsunaga, A., Ziemann, P., 2010. Gas-wall partitioning of organic compounds in a teflon film chamber and potential effects on reaction product and aerosol yield measurements. Aerosol Sci. Technol. 44, 881–892. https://doi.org/10.1080/02786826.2010.501044.
- McDonald, B.C., de Gouw, J.A., Gilman, J.B., Jathar, S.H., Akherati, A., Cappa, C.D., Jimenez, J.L., Lee-Taylor, J., Hayes, P.L., McKeen, S.A., 2018. Volatile chemical products emerging as largest petrochemical source of urban organic emissions. Science 359, 760–764.
- McMurry, P., Grosjean, D., 1985. Gas and aerosol wall losses in Teflon film smog chambers. Environ. Sci. Technol. 19, 1176–1182. https://doi.org/10.1021/es00142a006.
- McNeill, V., Woo, J., Kim, D., Schwier, A., Wannell, N., Sumner, A., Barakat, J., 2012. Aqueousphase secondary organic aerosol and organosulfate formation in atmospheric aerosols:

- a modeling study. Environ. Sci. Technol. 46, 8075–8081. https://doi.org/10.1021/es3002986.
- Nah, T., McVay, R.C., Zhang, X., Boyd, C.M., Seinfeld, J.H., Ng, N.L., 2016. Influence of seed aerosol surface area and oxidation rate on vapor wall deposition and SOA mass yields: a case study with α-pinene ozonolysis. Atmos. Chem. Phys. 16, 9361–9379.
- Ng, N.L., Chhabra, P.S., Chan, A.W.H., Surratt, J.D., Kroll, J.H., Kwan, A.J., McCabe, D.C., Wennberg, P.O., Sorooshian, A., Murphy, S.M., Dalleska, N.F., 2007. Effect of NOx level on secondary organic aerosol (SOA) formation from the photooxidation of terpenes. Atmos. Chem. Phys. 7 (19), 5159–5174.
- Odian, G., 2004. Principles of Polymerization. John Wiley & Sons.
- Odum, J., Hoffmann, T., Bowman, F., Collins, D., Flagan, R., Seinfeld, J., 1996. Gas/particle partitioning and secondary organic aerosol yields. Environ. Sci. Technol. 30, 2580–2585. https://doi.org/10.1021/es950943+.
- Pankow, J.F., 1994. An absorption model of the gas/aerosol partitioning involved in the formation of secondary organic aerosol. Atmos. Environ. 28, 189–193.
- Platts, J., Butina, D., Abraham, M., Hersey, A., 1999. Estimation of molecular linear free energy relation descriptors using a group contribution approach. J. Chem. Inf. Comput. Sci. 39, 835–845. https://doi.org/10.1021/ci980339t.
- Pöschl, U., 2005. Atmospheric aerosols: composition, transformation, climate and health effects. Angew. Chem. Int. Ed. 44, 7520–7540.
- Puzyn, T., Leszczynski, J., Cronin, M.T., 2010. Recent Advances in QSAR Studies: Methods and Applications. Springer Science & Business Media.
- Renbaum-Wolff, L., Grayson, J.W., Bateman, A.P., Kuwata, M., Sellier, M., Murray, B.J., Shilling, J.E., Martin, S.T., Bertram, A.K., 2013. Viscosity of α-pinene secondary organic material and implications for particle growth and reactivity. Proc. Natl. Acad. Sci. 110, 8014–8019.
- Salthammer, T., Goss, K.-U., 2019. Predicting the gas/particle distribution of SVOCs in the indoor environment using poly parameter linear free energy relationships. Environ. Sci. Technol. 53, 2491–2499.
- Seinfeld, J.H., Pandis, S.N., 2016. Atmospheric Chemistry and Physics: From Air Pollution to Climate Change. John Wiley & Sons.
- Shiraiwa, M., Ammann, M., Koop, T., Pöschl, U., 2011. Gas uptake and chemical aging of semisolid organic aerosol particles. Proc. Natl. Acad. Sci. 108, 11003–11008.
- Simoneit, B.R., 1989. Organic matter of the troposphere—V: application of molecular marker analysis to biogenic emissions into the troposphere for source reconciliations. J. Atmos. Chem. 8, 251–275.
- Tolocka, M., Jang, M., Ginter, J., Cox, F., Kamens, R., Johnston, M., 2004. Formation of oligomers in secondary organic aerosol. Environ. Sci. Technol. 38, 1428–1434. https://doi.org/10.1021/es035030r.
- Tsigaridis, K., Daskalakis, N., Kanakidou, M., Adams, P., Artaxo, P., Bahadur, R., Balkanski, Y., Bauer, S., Bellouin, N., Benedetti, A., 2014. The AeroCom evaluation and intercomparison of organic aerosol in global models. Atmos. Chem. Phys. 14, 10845–10895.
- Volkamer, R., Jimenez, J., San Martini, F., Dzepina, K., Zhang, Q., Salcedo, D., Molina, L., Worsnop, D., Molina, M., 2006. Secondary organic aerosol formation from anthropogenic air pollution: rapid and higher than expected. Geophys. Res. Lett. 33. https:// doi.org/10.1029/2006GL026899.
- Wexler, A.S., Seinfeld, J.H., 1990. The distribution of ammonium salts among a size and composition dispersed aerosol. Atmos. Environ. Part A 24, 1231–1246.
- Yeh, G., Ziemann, P., 2014. Alkyl nitrate formation from the reactions of C-8-C-14 nalkanes with OH radicals in the presence of NOx: measured yields with essential corrections for gas-wall partitioning. J. Phys. Chem. A 118, 8147–8157. https://doi.org/ 10.1021/ip500631v.
- Yeh, G., Ziemann, P., 2015. Gas-wall partitioning of oxygenated organic compounds: measurements, structure-activity relationships, and correlation with gas chromatographic retention factor. Aerosol Sci. Technol. 49, 726–737. https://doi.org/10.1080/02786826.2015.1068427.
- Zhang, H., Chen, G., Hu, J., Chen, S.-H., Wiedinmyer, C., Kleeman, M., Ying, Q., 2014a. Evaluation of a seven-year air quality simulation using the weather research and forecasting (WRF)/community multiscale air quality (CMAQ) models in the eastern United States. Sci. Total Environ. 473, 275–285.
- Zhang, X., Cappa, C., Jathar, S., Mcvay, R., Ensberg, J., Kleeman, M., Seinfeld, J., 2014b. Influence of vapor wall loss in laboratory chambers on yields of secondary organic aerosol. Proc. Natl. Acad. Sci. U. S. A. 111, 5802–5807. https://doi.org/10.1073/pnas.1404727111.
- Zhou, C., Jang, M., Yu, Z., 2019. Simulation of SOA formation from the photooxidation of monoalkylbenzenes in the presence of aqueous aerosols containing electrolytes under various NO x levels. Atmos. Chem. Phys. 19, 5719–5735.
- Zuend, A., Marcolli, C., Booth, A., Lienhard, D.M., Soonsin, V., Krieger, U., Topping, D.O., McFiggans, G., Peter, T., Seinfeld, J.H., 2011. New and extended parameterization of the thermodynamic model AlOMFAC: calculation of activity coefficients for organic-inorganic mixtures containing carboxyl, hydroxyl, carbonyl, ether, ester, alkenyl, alkyl, and aromatic functional groups. Atmos. Chem. Phys. 11, 9155–9206.